ACCSCIENCE PUBLISHING

International Journal of Bioprinting

RESEARCH ARTICLE

Rheology-informed hierarchical machine learning model for the prediction of printing resolution in extrusion-based bioprinting

Dageon Oh[1], Masoud Shirzad[1], Min Chang Kim[2], Eun-Jae Chung[3], and Seung Yun Nam[1,2]*

[1]Industry 4.0 Convergence Bionics Engineering, Pukyong National University, Busan 48513, Republic of Korea

[2]Major of Biomedical Engineering, Division of Smart Healthcare, Pukyong National University, Busan 48513, Republic of Korea

[3]Department of Otorhinolaryngology-Head and Neck Surgery, Seoul National University College of Medicine, Seoul 03080, Republic of Korea

Abstract

In this study, a rheology-informed hierarchical machine learning (RIHML) model was developed to improve the prediction accuracy of the printing resolution of constructs fabricated by extrusion-based bioprinting. Specifically, the RIHML model, as well as conventional models such as the concentration-dependent model and printing parameter-dependent model, was trained and tested using a small dataset of bioink properties and printing parameters. Interestingly, the results showed that the RIHML model exhibited the lowest error percentage in predicting the printing resolution for different printing parameters such as nozzle velocities and pressures, as well as for different concentrations of the bioink constituents. Besides, the RIHML model could predict the printing resolution with reasonably low errors even when using a new material added to the alginate-based bioink, which is a challenging task for conventional models. Overall, the results indicate that the RIHML model can be a useful tool to predict the printing resolution of extrusion-based bioprinting, and it is versatile and expandable compared to conventional models since the RIHML model can easily generalize and embrace new data.

Keywords: Bioprinting; Printability; Machine learning; Rheology; Printing resolution

***Corresponding author:**
Seung Yun Nam
(synam@pknu.ac.kr)

Citation: Oh D, Shirzad M, Kim MC, *et al*., 2023, Rheology-informed hierarchical machine learning model for the prediction of printing resolution in extrusion-based bioprinting. *Int J Bioprint*, 9(6): 1280.
https://doi.org/10.36922/ijb.1280

Received: March 16, 2023
Accepted: July 13, 2023
Published Online: August 9, 2023

1. Introduction

In recent times, additive manufacturing approaches including three-dimensional (3D) bioprinting have emerged as essential tools for fabricating artificial tissue and organ constructs. Specifically, compared to conventional biofabrication methods, the 3D bioprinting technique can effectively deposit bioink layer by layer with a designed combination of biomaterials and living cells in desired locations and patterns[1-5]. The primary bioprinting methods include inkjet-based bioprinting, extrusion-based bioprinting, and laser-assisted bioprinting[6-9]. Among them, extrusion-based bioprinting has been the most widely used technique for research and commercial purposes. This is

principally due to the availability of a wide range of usable material viscosity, which allows for freedom in material selection when preparing bioink[10-16].

However, the advantages of the generous availability of bioink candidates including hydrogels, extracellular matrix, bioceramic particles, and shear thickening materials create difficulties in tuning bioink compositions and finding appropriate printing conditions[17,18]. Thus, to overcome these challenges and complexities in the preparation of bioinks and extrusion-based bioprinting, printability has recently attracted considerable attention. Although the definition of printability in extrusion-based bioprinting is still in discussion, it is obvious that better printability can improve the printing accuracy and shape fidelity of the printed constructs, leading to faster fabrication speed and long-term stable functionality[19-22]. Further, recent printability studies have quantitatively evaluated printing accuracy and shape fidelity using the assessment of various outcomes, such as printing resolution relative to the nozzle diameter, distance between filaments, pore size and shape in a grid structure, and height of the stacked layers[23-25]. In addition, these studies have demonstrated that printability is deeply linked to how to control the rheological properties of bioinks (viscosity, shear modulus, and gelation) and the printing parameters (printing pressure, temperature, nozzle size, nozzle length, and nozzle velocity)[26-32]. However, it is still difficult to find the optimal printing conditions because the assessment of the printability often relies on trial and error with a repeated change of the bioink composition and printing parameters, which is time-consuming and cost-ineffective.

Hence, printability prediction is critical to the accurate and effective fabrication of tissue-engineered constructs using the extrusion-based bioprinting technique. In several existing studies, the physical model-based computation was adopted for printability prediction[33-38]. More precisely, the physical model of printability prediction was derived from hydrodynamic equations combined with the rheological modeling of generalized Newtonian fluid, mainly power-law fluid. Using the physical model, the printing resolution of the output filament was simulated with multiple printing parameters and compared with the actual printing resolution. Although several studies using the physical model reported interesting results, the model holds many assumptions and simplifications, limiting its application in various bioprinting tasks. For instance, the physical prediction model is highly sensitive to the power law index, which can be obtained by the line fitting of the measured viscosity. Thus, small errors in rheological measurement and line fitting may have a significant effect on prediction accuracy. Additionally, the assumptions in the physical model, such as the incompressibility of bioink and the ideal pressure drop in the system, may not coincide with reality; hence, the accumulated errors can cause a gap between the predicted and actual results.

Recently, multiple studies of printability prediction using machine learning have been reported to overcome the limitations of physical models. Besides, due to the time-consuming and sequential bioprinting procedure from bioink preparation to 3D deposition, the size of the acquired dataset is relatively small. Therefore, most of these studies employed simple supervised machine learning methods, such as support vector machine, decision tree, lasso regression, and ridge regression, to estimate printing resolution with the confined variation of bioink composition and printing parameters[39-43]. Specifically, a few studies employed artificial neural networks for printability prediction, but its architecture is hardly deep with shallow hidden layers and a limited number of neurons because of the dataset size[44-46]. Moreover, in most of the neural network-based printability prediction models, superficial parameters such as the concentration of each bioink component were used in the input layer of the artificial neural network. This may significantly limit the expandability of the machine learning model since the neural network should be rebuilt and newly trained for every change in the bioink composition. Therefore, an improved machine learning model, which is versatile with various bioink combinations and penetrates the essence of bioprinting with profoundly related parameters, is required.

Furthermore, the rheological properties, such as viscosity and shear modulus, of bioinks have been verified to be closely related to the printing parameters to optimize the printability of extrusion-based bioprinting (Figure 1)[47-53]. For instance, even though the viscosity of bioink increases, the flow rate can be maintained if the printing parameters such as pressure and nozzle size are appropriately increased. Even with the same flow rate, the printing resolution significantly correlates with the shear modulus and nozzle velocity. Despite the deep correlation between rheology and printability, there have been no studies that actively applied rheological measurements of various bioinks and multiple printing parameters to machine learning.

Therefore, in this study, a rheology-informed hierarchical machine learning (RIHML) model was developed to predict printability in extrusion-based bioprinting. Among previously suggested methods to quantify printability, the assessment of printing resolution, which has been widely applied in numerous printability studies, was mainly adopted. To construct a dataset for training the models, the optical images of printed scaffolds

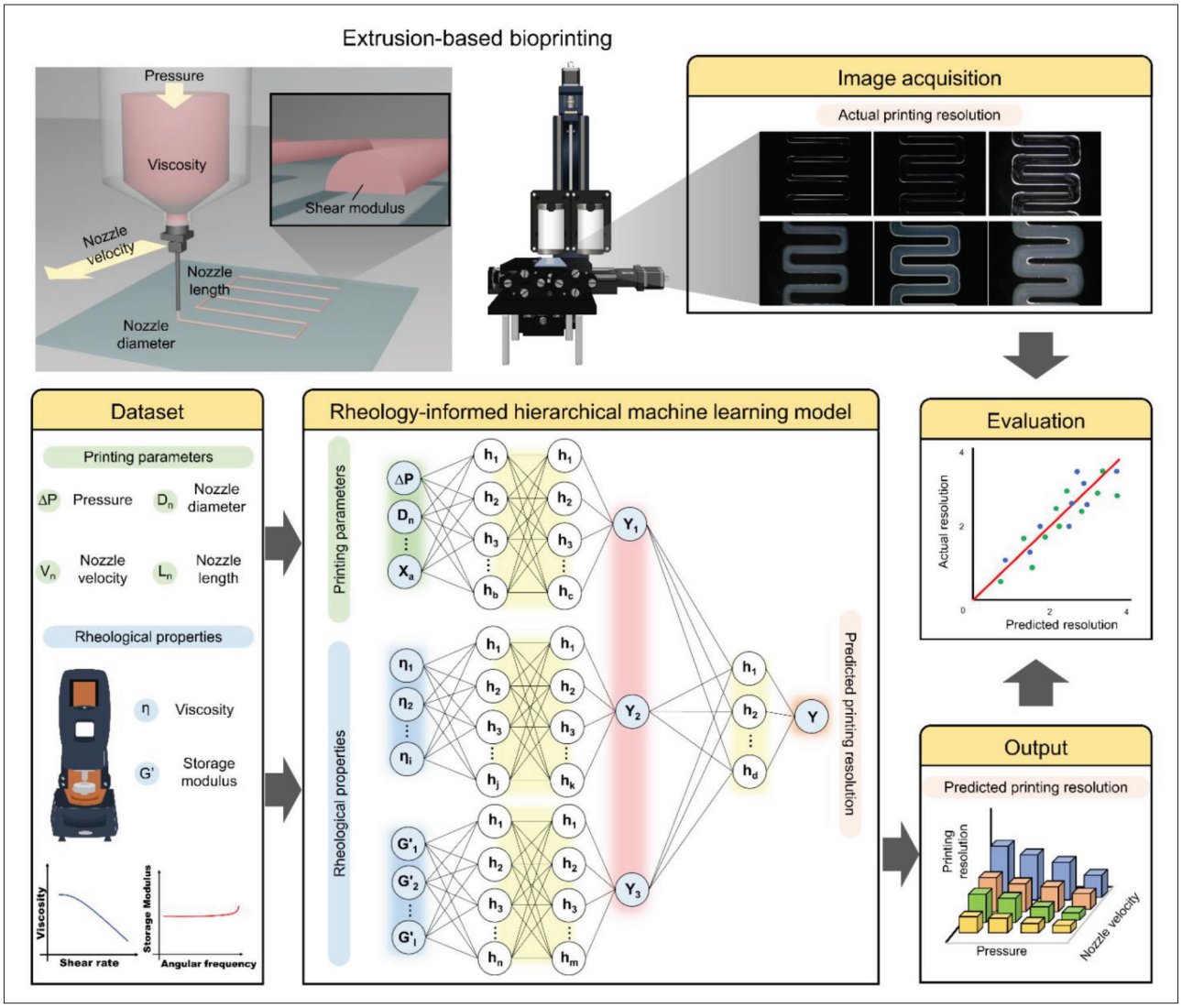

Figure 1. Overview of the process of the prediction of printing resolution based on a rheology-informed hierarchical machine learning model.

were collected with various printing conditions and bioink concentrations on a digital microscope. The acquired image was processed to quantify the printing resolution using an automated program to calculate strand size. In addition, the assessed viscosity and storage modulus were used as a rheological dataset to construct the input layers of a multi-input neural network combined with the printing parameters. Thus, the RIHML model, as well as the conventional models such as the concentration-dependent machine learning (CDML) model and printing parameter-dependent machine learning (PDML) model, was trained and tested using a small dataset of bioink properties and printing parameters. After model training, the prediction accuracy using each machine learning model was verified and compared for different printing parameters, such as nozzle velocities and pressures, as well as for different concentrations of bioink constituents. In addition, printing resolution was assessed using a new material added to the alginate-based bioink, to examine the feasibility of the RIHML as a versatile and expandable tool to predict the printing accuracy in extrusion-based bioprinting.

2. Materials and methods

2.1. Bioink preparation

In this study, ten bioinks were prepared using three base hydrogels and three additives as shown in Table 1. Precisely, Pluronic F-127 (F127, Sigma-Aldrich) was used as the base material without additives. Particularly, it was dissolved in deionized water at 4°C and prepared with three concentrations of 35%, 40%, and 45%. Another base bioink material, gelatin (porcine skin-derived, Sigma-Aldrich),

Table 1. Different types of bioink and their compositions in weight percentage

Formulation	F127 (%)	Alginate (%)	$CaCl_2$ (%)	CNC (%)	Gelatin (%)	XG (%)
F127 35%	35	0	0	0	0	0
F127 40%	40	0	0	0	0	0
F127 45%	45	0	0	0	0	0
Gelatin 10%/XG 2%	0	0	0	0	10	2
Gelatin 5%/XG 3%	0	0	0	0	5	3
Gelatin 10%/XG 4%	0	0	0	0	10	4
Alginate 2%/$CaCl_2$ 0.2%	0	2	0.2	0	0	0
Alginate 2%/$CaCl_2$ 0.3%	0	2	0.3	0	0	0
Alginate 2%/CNC 2.5%	0	2	0	2.5	0	0
Alginate 2%/CNC 5%	0	2	0	5	0	0

Abbreviations: CNC, cellulose nanocrystal; XG, xanthan gum.

was mixed homogeneously with xanthan gum (XG, Sigma-Aldrich) in three concentrations of 2%, 3%, and 4% in a planetary centrifugal mixer (AR-100, Thinky). Additionally, sodium alginate (Sigma-Aldrich) was used as a base material, and it was crosslinked by calcium chloride ($CaCl_2$, Sigma-Aldrich) with two concentrations of 0.2% and 0.3%, to increase the viscosity. Specifically, the sodium alginate and $CaCl_2$ were mixed at a ratio of 7:3 using a three-way stopcock, and the final concentration of the alginate solution was 2%. Furthermore, cellulose nanocrystal (CNC, CelluForce) was utilized to improve the rheological properties of the alginate-based bioink. To prepare the sodium alginate/CNC composite bioink, sodium alginate solution was mixed with dispersed CNCs in deionized water using the planetary centrifugal mixer, and the final concentrations of CNC were 2.5% and 5%, respectively.

2.2. Rheological characterization

The rheological properties of the bioinks were measured using a rotational rheometer (HR-2, TA Instruments) with a 20 mm parallel plate at a gap distance of 1000 μm. In addition, the printing temperature of the gelatin-based bioink was estimated by a temperature sweep test, which measured the storage modulus and loss modulus at an angular frequency of 10 rad/s. Specifically, for the flow sweep test, the shear rate was increased from 0.1 to 1000 1/s at 23°C for alginate-based and Pluronic-F127 bioinks. For gelatin-based bioinks, the temperature was set to 35°C to enhance printability. Following the amplitude sweep to determine the appropriate strain, the frequency sweep test was conducted to evaluate storage modulus within a specific angular frequency range. Specifically, the test commenced at 0.1 rad/s and concluded at 500 rad/s with the same temperatures as in the flow sweep test and a strain of 1% for each bioink.

2.3. Bioprinting

In this study, all bioinks were printed with the same one-layer scaffold structure. More precisely, the structure was designed with physical dimensions of 12 × 24 mm and a strand-to-strand distance of 4 mm. Specifically, all the scaffolds were fabricated at the same distance of 0.4 mm between the nozzle tip and the printing plate. Furthermore, two types of nozzles, i.e., 21G (inner diameter: 514 μm) and 23G (inner diameter: 337 μm) with multiple lengths (L: 2.54 cm in length for 21G and 23G; S: 1.27 cm in length for 21G), were used to print the scaffolds. Additionally, the Pluronic-F127 and sodium alginate-based bioinks were printed at room temperature (23°C), and the gelatin-based bioinks were printed at a temperature of 35°C, which was the same as the rheological characterization. Moreover, four different values of the nozzle velocity (speed of printer head movement), including 1, 2, 4, and 8 mm/s, were examined in the bioprinting process. Due to the differences in viscosity and yield strength of the bioinks, the printing pressure was adjusted depending on the extrudability of each bioink at a pressure range between 10 and 350 kPa.

2.4. Data acquisition

The processes of printing and rheological data acquisition for the prediction of printing resolution are described in Figure 2A. In the first step, bioinks with different compositions and concentrations (F127, gelatin/XG, alginate/$CaCl_2$, and alginate/CNC) were prepared; afterward, measurement of the rheological properties and printing of scaffolds were performed, respectively. Specifically, structures were fabricated in the extrudable range of each bioink with a designated path. Precisely, scaffolds were printed with five-center lines, and images were taken and saved by a digital microscope in 2592 × 1944 pixels. Except for a reference line, four lines were evaluated in the images to calculate the printing resolution

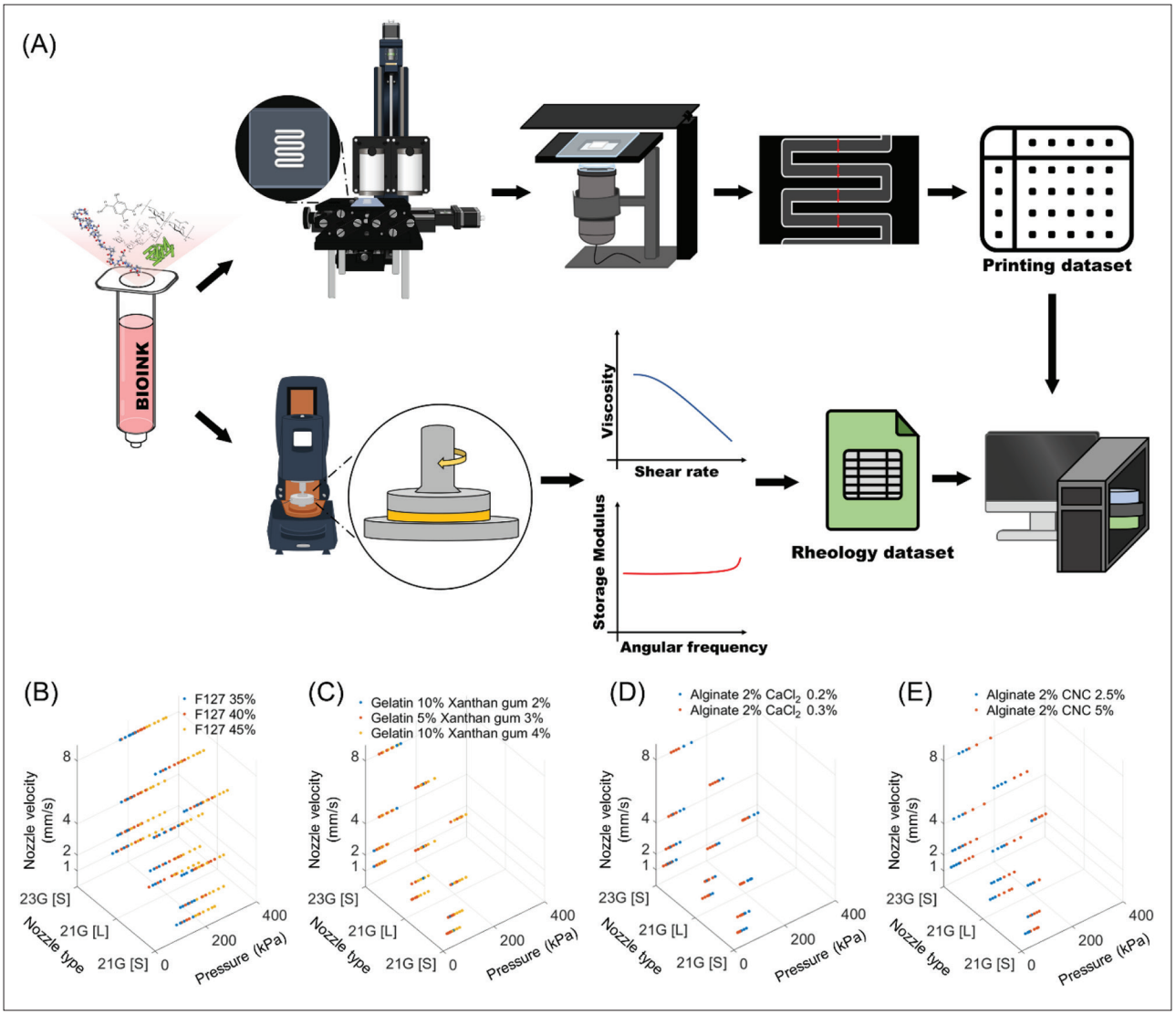

Figure 2. (A) Process of data acquisition: investigation of printing resolution and rheological assessment. 3D graphs of the collected data with printing parameters for the bioink compositions of (B) F127, (C) gelatin/xanthan gum, (D) alginate/$CaCl_2$, and (E) alginate/CNC composite.

using the algorithm to measure the strand size, as shown in **Figure S1** (Supplementary File). In particular, the algorithm was composed of two main steps. The first step was finding the path line, which can decrease errors by a missed detection of the line. Afterward, the image was changed to grayscale, and a position where the centers of the maximum signals on each line matched the printing path was found. The second step was to quantify the average strand size. Specifically, the image was reconstructed to a binary one and cropped with white pixels to leave 2 mm from the center lines to each side. Particularly, nine lines in the cropped image were selected using a projection grade of white pixels. Specifically, when the path and the selected lines were matched up, the average strand size of the scaffolds was calculated. The information on material concentration, printing pressure, nozzle diameter, nozzle length, nozzle velocity, and printing resolution was stored in the printing dataset. Furthermore, to create a sub-dataset for the rheological properties, 41 values of measured viscosity and 21 values of storage modulus data were acquired at the angular frequency region from 0.1 to 10 rad/s and subsequently, saved with bioink information.

2.5. Machine learning model

This study utilized two classical machine learning algorithms (random forest [RF] and support vector machine [SVM]), two conventional machine learning models (printing parameter-dependent machine learning model [PDML] and concentration-dependent machine learning model [CDML]), and a developed multi-input machine learning

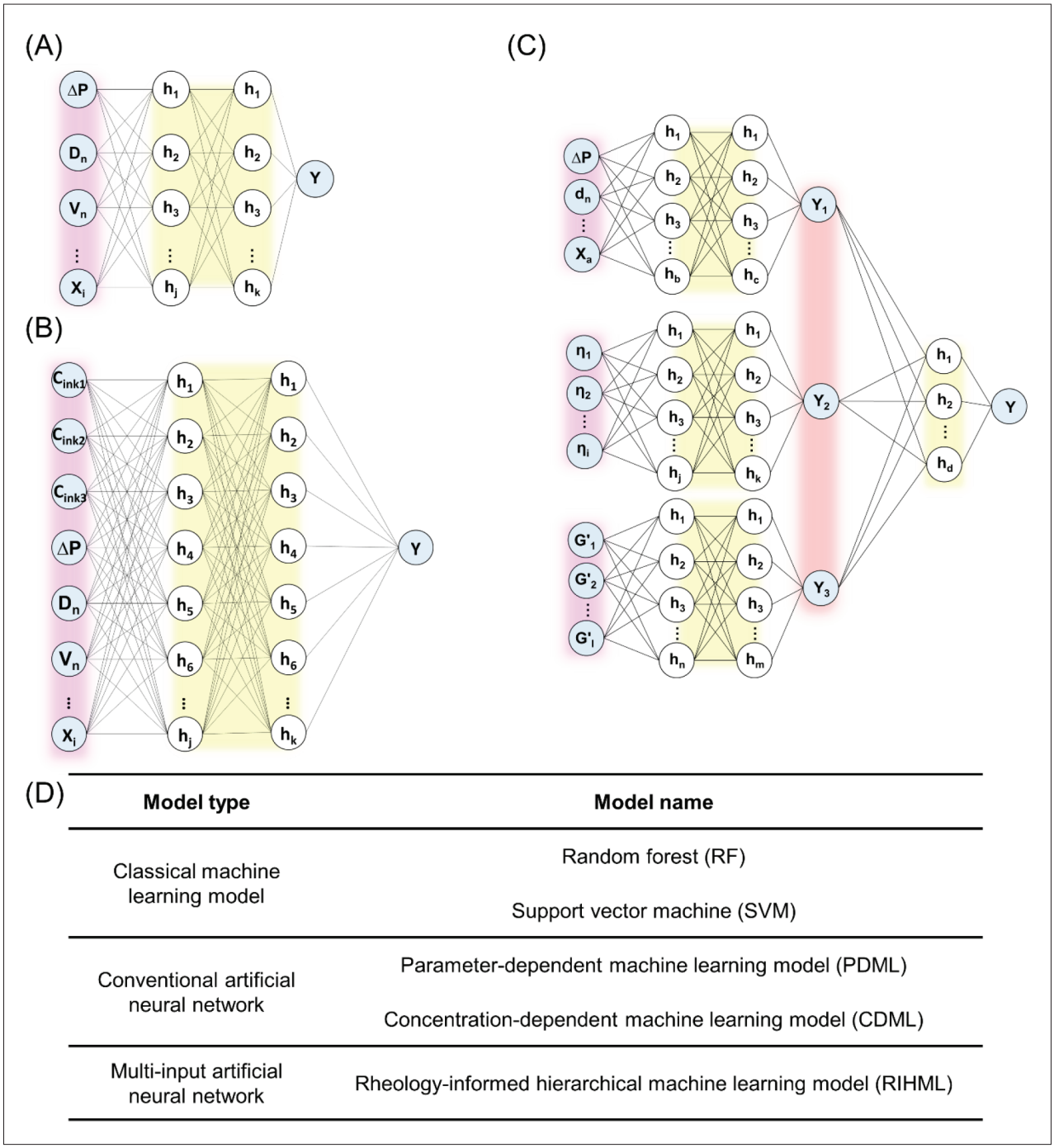

(D)

Model type	Model name
Classical machine learning model	Random forest (RF)
	Support vector machine (SVM)
Conventional artificial neural network	Parameter-dependent machine learning model (PDML)
	Concentration-dependent machine learning model (CDML)
Multi-input artificial neural network	Rheology-informed hierarchical machine learning model (RIHML)

Figure 3. Structure of artificial neural network-based models: (A) the parameter-dependent machine learning model, (B) the concentration-dependent machine learning model, and (C) the rheology-informed hierarchical machine learning model. (D) Table of the machine learning model types and corresponding model names.

model (rheology-informed hierarchical machine learning model [RIHML]) to predict the printing resolution using regression as shown in Figure 3D. Two representative classical machine learning algorithms, RF and SVM, were implemented using the sci-kit learn package in Python. Additionally, the Keras module from TensorFlow was used to develop the artificial neural network-based models, which specifically consisted of rectified linear unit (ReLU) function with the same hyperparameters, such as batch size and epoch. Furthermore, the train set, validation set,

and test set split by the ratio of 6:2:2 were performed with an applied random seed and fixed to all the models to avoid overfitting and estimate learning performance. To assess the performance of learning, mean squared error (MSE) was used for loss estimation.

Specifically, two classical machine learning algorithms, RF and SVM, were prepared based on conventional regression models using ensembles of multiple decision trees and hyperplanes with maximum margin, respectively. Moreover, the two conventional machine learning models consisted of an input layer, hidden layers, and an output layer as shown in Figure 3A and B. Specifically, the printing parameter-dependent machine learning model uses only printing parameters, such as printing pressure, nozzle velocity, nozzle diameter, and nozzle length. Besides, the concentration-dependent machine learning model was incorporated into the input layer consisting of the printing parameters and the concentrations of each bioink material.

Additionally, the RIHML was used with a multi-input layer model consisting of three input layers with hidden layers, concatenated layer, and its hidden layer; and an output layer shown in Figure 3C. The rheological properties, such as the viscosity and storage modulus, were used as the first and second input layers of the RIHML, respectively; and the last input layer consisted of the printing parameters. The hidden layers of each input layer were calculated separately and concatenated with the output layer. The final output was derived with a second hidden layer whose input is the concatenated output of the first hidden layer.

2.6. Prediction of the printing resolution

The machine learning models predicted the printing resolution with different cases involving new printing parameters, different concentrations, and different bioink compositions. More particularly, a dataset was created by multiple compositions of F127, gelatin/XG, and alginate/$CaCl_2$. Splitting was employed to train the model, except for the variable required to perform the prediction in the pre-training stage. Specifically, the independent datasets in the pre-training stage were provided for each machine learning model. They were divided into three parts (training set, validation set, and testing set) to train the model and estimate learning performance. The trained models have predicted printing resolution with a dataset consisting of excluded variables in the training dataset. The error criterion evaluating printing resolution accuracy was evaluated using Equation I.

$$\text{Error}(\%) = \frac{|\text{AR} - \text{PR}|}{\text{AR}} \times 100 \quad \text{(I)}$$

where AR is the actual printing resolution and PR is the predicted printing resolution. This represents the difference between the actual and predicted value. Moreover, four different nozzle velocities and five unequal pressure values were used as the variables of the printing parameters to predict the printing resolution with two conventional machine learning models and the RIHML. Specifically, the printing resolution was predicted by different material concentrations of bioinks with a split dataset via CDML and RIHML. Additionally, a new composition, alginate/CNC composite bioink, was used to investigate the possibility of predicting the novel materials not considered in the training set with CDML and RIHML. In the case of CDML, the number of input layer neurons correlate with the number of materials. It means that by adding a new material, parameters of the new material, such as concentration, should be included in the input layer, thus increasing the neurons. To follow the previous structure, the neuron of the CNC existed in the input layer of CDML.

In addition, to provide a visual representation, binary images of the printed scaffolds were created using simulation. To generate the binary image, the printing strand size obtained from the machine learning model was converted into pixels. Using the converted strand size, the single-pixel lines representing the actual printing path were dilated considering printing directions and angles. Afterward, the resulting binary values were converted to the binary image to accurately simulate the printed scaffolds based on the predicted printing strand size.

3. Results

3.1. Rheological properties of hydrogels

In this study, the viscoelastic properties including viscosity and storage modulus were assessed and implemented into a rheological dataset of the bioinks. As shown in Figure 4A, the viscosity for ten bioinks was prepared to compare the viscoelastic properties. Specifically, the shear-thinning behavior was observed in the flow curves of all bioinks, and the F127-based bioinks exhibited the highest viscosity compared to other bioinks. The flow curves of gelatin- and alginate-based bioinks are relatively low and partially overlapped while increasing shear rates. Consequently, the viscosities for various bioinks were compared with each other at the shear rate of 100 1/s as shown in Figure 4B. The storage modulus was also measured to investigate the mechanical strength of the bioinks (Figure 4C and D). Similar to the viscosity assessment, the highest shear moduli were shown with the F127-based bioink. Additionally, viscosities and storage moduli of gelatin- and alginate-based bioinks were correlated with the increasing concentration of gelatin/XG and CNC, respectively. However, while the shear moduli of alginate-based bioinks crosslinked with

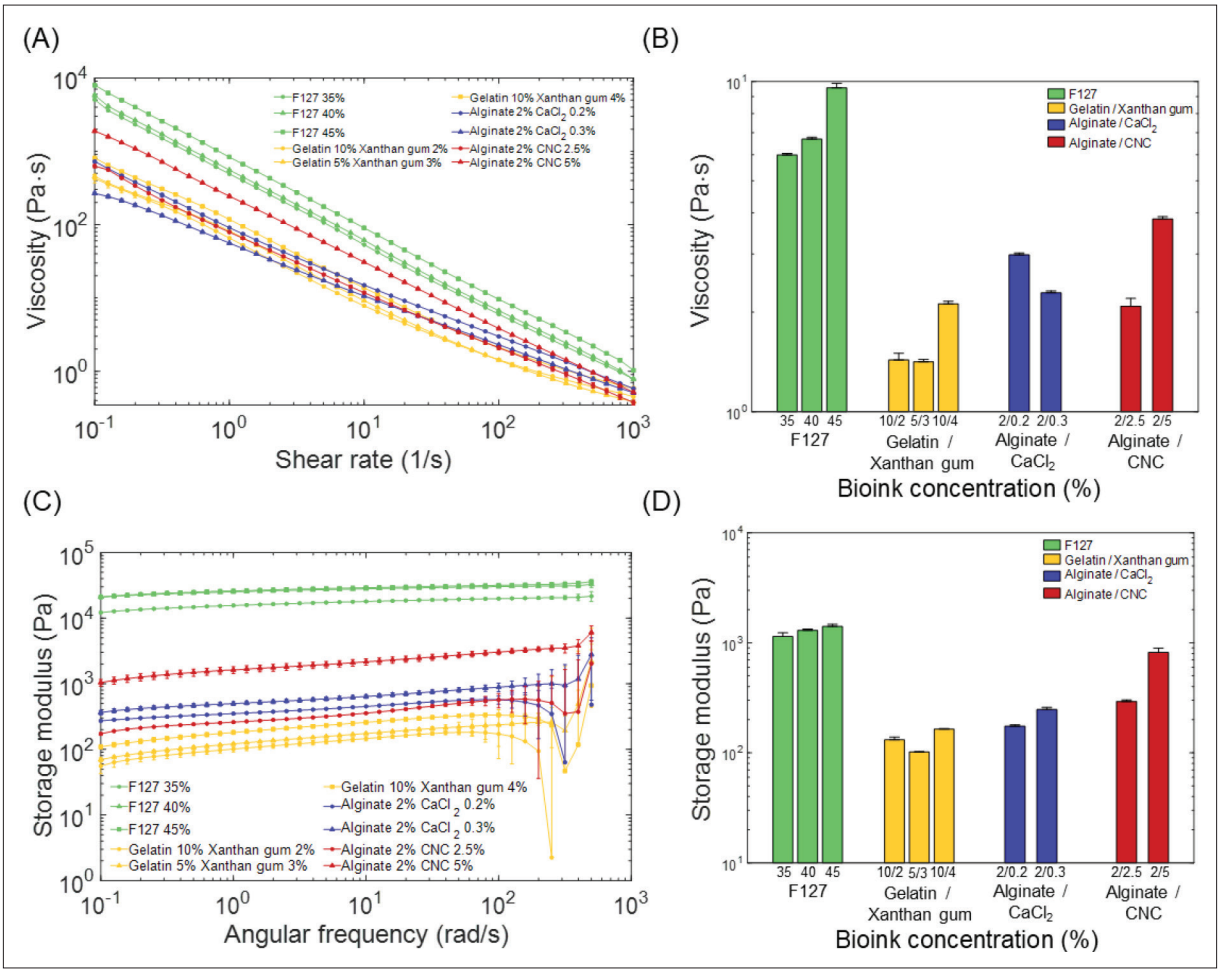

Figure 4. Rheological properties of the bioinks. (A) Viscosity and (C) storage modulus of the bioinks of F127, gelatin/xanthan gum, alginate/$CaCl_2$, and alginate/CNC. (B) Viscosity at a specific shear rate of 100 1/s and (D) storage modulus at a specific angular frequency of 100 rad/s.

$CaCl_2$ were increased with the concentration of $CaCl_2$, their viscosities decreased as the concentration of $CaCl_2$ increased. Overall, the dataset of rheological properties was collected for each composition with 41 and 21 values of viscosity data and storage moduli, respectively.

3.2. Printing data acquisition

A self-developed imaging setup and algorithm were used to identify and quantify the printing strand size in the microscopic images. Specifically, the printing resolution was evaluated based on the quantified strand size ranging from 0 to 4 mm. All the bioinks were printed with various pressures, four velocities, and three nozzle types as shown in Figure 2B and **Figure S3** (Supplementary File). The range of the pressure for printing the bioinks was from 10 to 350 kPa. Furthermore, for each nozzle velocity, about 110 data were investigated to figure out the printing quality. In total, 537 printing resolution data were accumulated by 10 compositions of bioinks. Specifically, 72, 47 to 49, 45 to 47, and 41 to 44 data were collected with F127, gelatin/XG, alginate/$CaCl_2$, and alginate/CNC, respectively, as presented in **Table S1** (Supplementary File).

3.3. Machine learning

In this study, the learning performance of the machine learning models was verified using the collected datasets of printing resolution. Specifically, they were divided into a training set and a test set, as shown in Figure 5A and B. **Figure S4A–C** (Supplementary File) present the training loss and validation loss in the learning curve at 300 epochs for PDML, CDML, and RIHML. Generally, after successful training, the training loss was lower than the validation loss. The rheology-informed model exhibited the lowest training loss of 0.05 and validation loss of 0.08 compared with the training loss of 0.08 and validation loss of 0.13 in the concentration-dependent model, which was similar to the tendency often seen in successful training. Nevertheless, training using the parameter-dependent model was not effective with a higher training loss of 0.68 than the validation set loss of 0.62. Additionally,

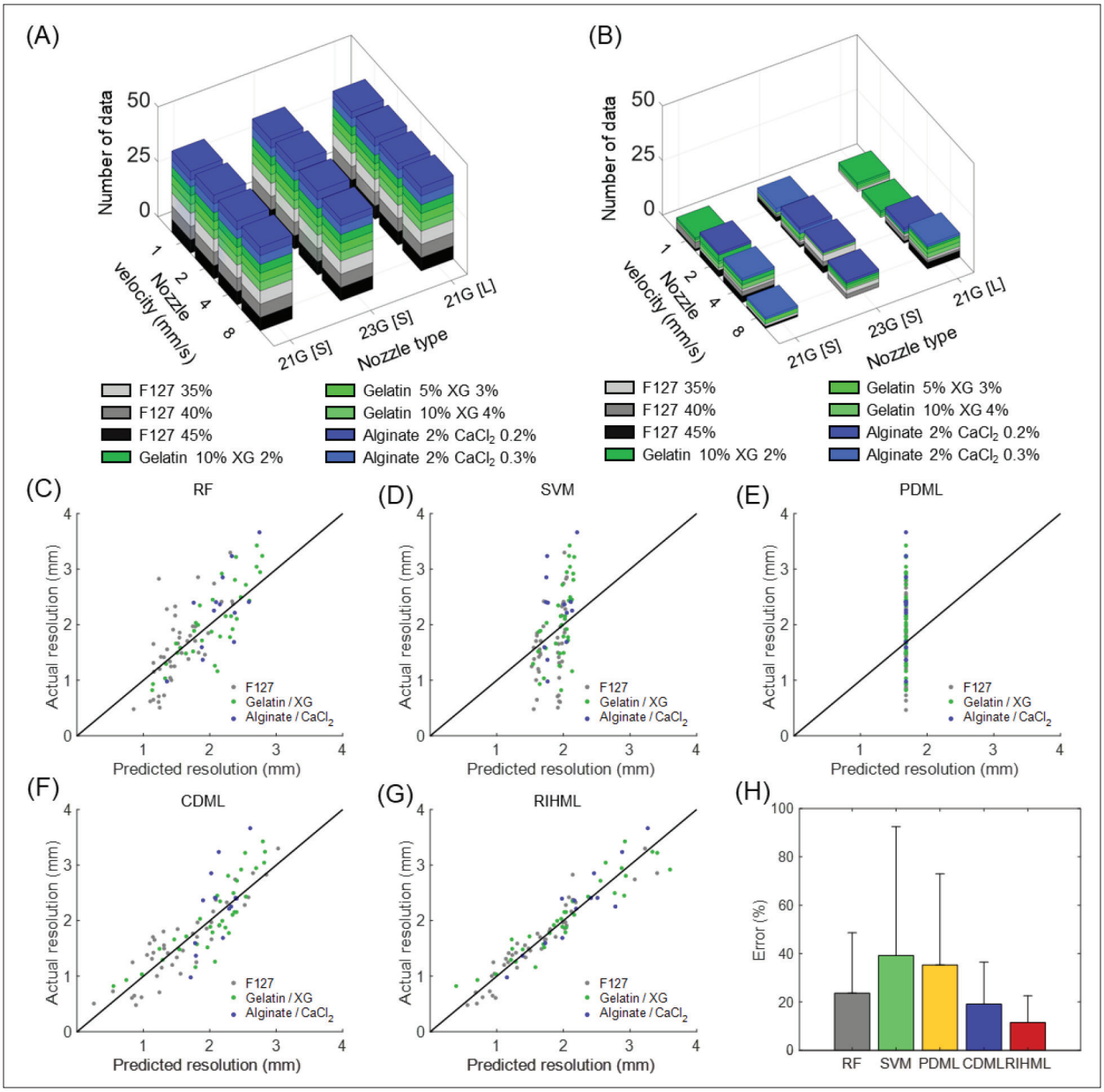

Figure 5. 3D-stacked bar graphs with printing parameters for (A) full dataset and (B) test dataset with the bioinks of F127, gelatin/xanthan gum, and alginate/$CaCl_2$. Fitting actual values with prediction values with (C) random forest (RV), (D) support vector model (SVM), (E) parameter-dependent machine learning (PDML) model, (F) concentration-dependent machine learning (CDML) model, and (G) rheology-informed hierarchical machine learning (RIHML) model. (H) Bar graph of average errors for each model.

as shown in Figure 5E, the PDML predicted every test resolution to be 1.68 mm, which does not match the actual values ranging from 0 to 4 mm while other artificial neural network models showed reasonable fitting results (Figure 5F and G). The experimental results from the RF model had a large standard deviation of errors as shown in Figure 5C, indicating that the prediction was significantly biased. Furthermore, prediction accuracy using another classical machine learning model, SVM, showed a similar trend with PDML, resulting in inadequate fitting as depicted in Figure 5D. These models also exhibited large errors of approximately 40%, as described in bar graphs in Figure 5H. As a result, the prediction of two classical machine learning models and PDML imply that it is not appropriate for forecasting the printing resolution of various bioink types. Furthermore, the predicted resolution of the rheology-informed model most accurately matched the actual printing resolution.

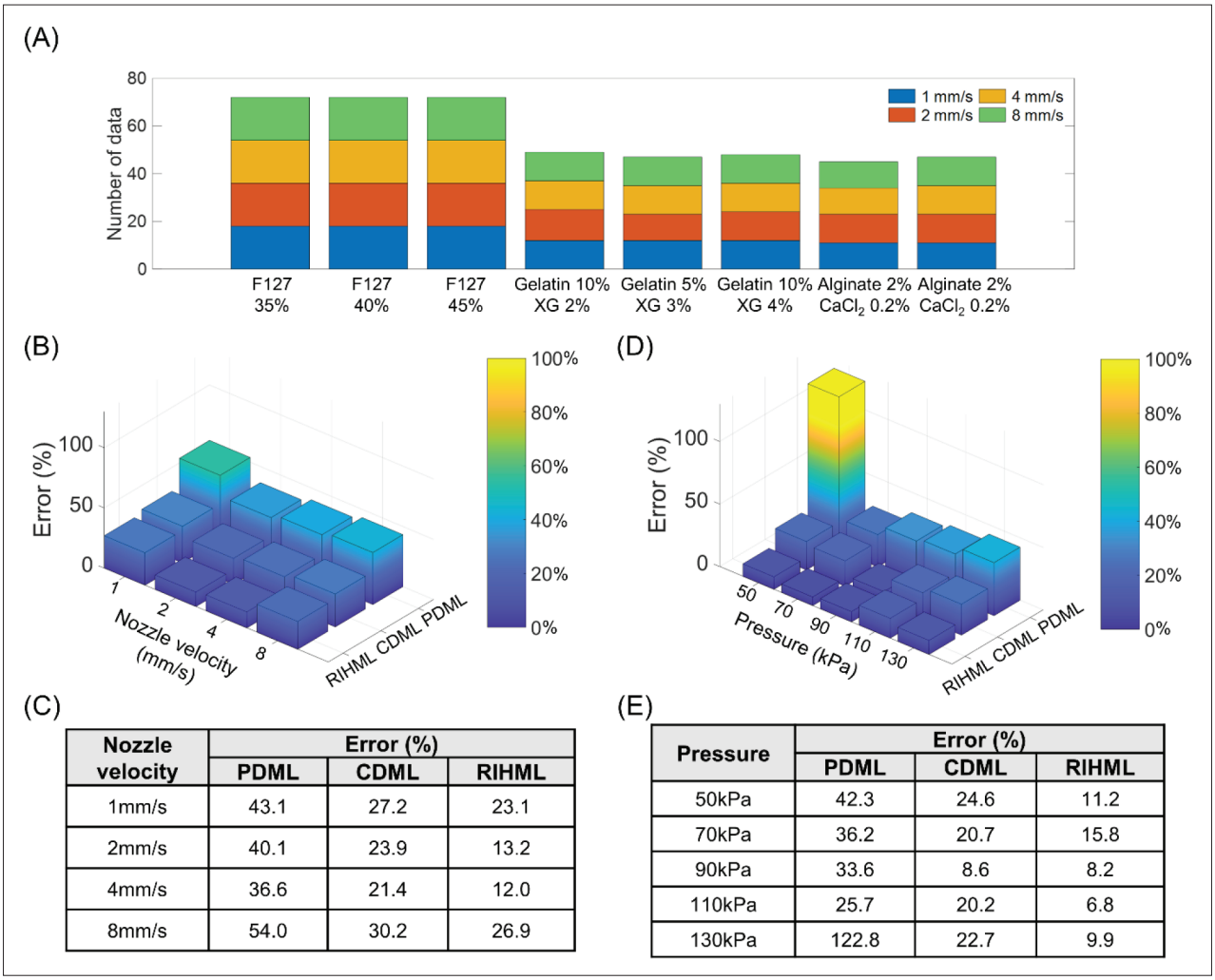

Nozzle velocity	Error (%)		
	PDML	CDML	RIHML
1mm/s	43.1	27.2	23.1
2mm/s	40.1	23.9	13.2
4mm/s	36.6	21.4	12.0
8mm/s	54.0	30.2	26.9

Pressure	Error (%)		
	PDML	CDML	RIHML
50kPa	42.3	24.6	11.2
70kPa	36.2	20.7	15.8
90kPa	33.6	8.6	8.2
110kPa	25.7	20.2	6.8
130kPa	122.8	22.7	9.9

Figure 6. (A) Stacked bar graph of the amount of data for different materials and nozzle velocities. (B) 3D bar graph and (C) table of calculated errors in various nozzle velocities (1, 2, 4, and 8 mm/s) and different machine learning models (PDML, CDML, and RIHML). (D) 3D bar graph and (E) table of calculated errors in various pressures (50, 70, 90, 110, and 130 kPa) with different machine learning models (PDML, CDML, and RIHML). Abbreviations: CDML, concentration-dependent machine learning; RIHML, rheology-informed hierarchical machine learning; PDML, parameter-dependent machine learning.

3.4. Prediction of printing resolution

3.4.1. Prediction with new printing parameters

Three machine learning models were compared to predict printing resolution using different parameters, including nozzle velocity and pressure. Particularly, the same datasets were used to train and predict each machine learning model as described in Figure 6A and **Table S1** (Supplementary File). As shown in Figure 6B and C, all errors have a similar trend when nozzle velocity was used as a variable of bioprinting. Descriptively, when the velocity was 4 mm/s, the errors were lowest and equal to 36.6%, 21.4%, and 12.0% for PDML, CDML, and RIHML, respectively; however, by increasing the velocity to 8 mm/s, the errors rose to 54%, 30.2%, and 26.9% for PDML, CDML, and RIHML, respectively. The prediction results with different nozzle velocities indicate that the rheology-informed machine learning model exhibited the lowest error (18.8% on average) among all models. Furthermore, errors in the prediction of printing resolution with various pressures (50, 70, 90, 110, and 130 kPa) using the machine learning models are illustrated in Figure 6D and E. RIHML could predict the printing resolution with the lowest error (10.38% on average), which is 2-fold and 5-fold lower than CDML and PDML, respectively. The highest error in the PDML model was around 123% in 130 kPa, demonstrating an approximately 13-fold error using RIHML at the same condition.

3.4.2. Prediction with different concentrations of bioink components

Due to the neural network structure of the PDML, it is hardly used for varying concentrations of bioink. Thus,

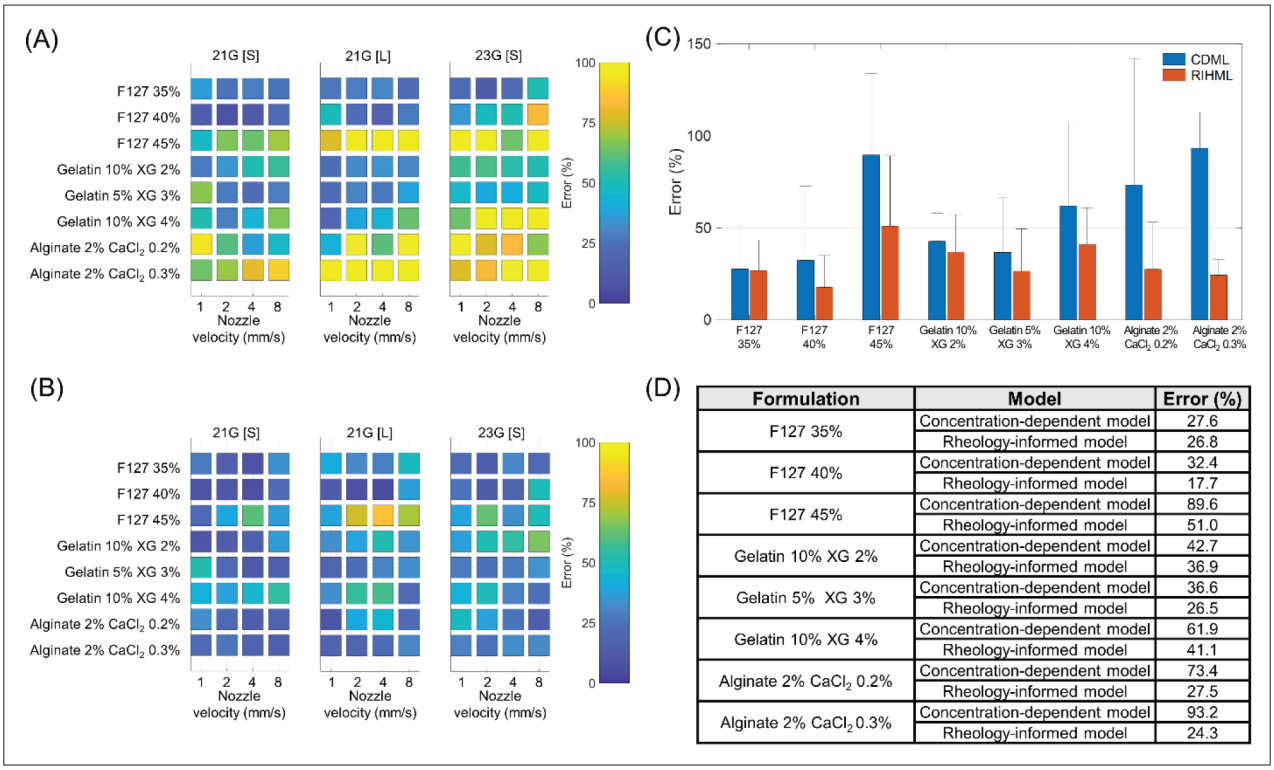

Formulation	Model	Error (%)
F127 35%	Concentration-dependent model	27.6
	Rheology-informed model	26.8
F127 40%	Concentration-dependent model	32.4
	Rheology-informed model	17.7
F127 45%	Concentration-dependent model	89.6
	Rheology-informed model	51.0
Gelatin 10% XG 2%	Concentration-dependent model	42.7
	Rheology-informed model	36.9
Gelatin 5% XG 3%	Concentration-dependent model	36.6
	Rheology-informed model	26.5
Gelatin 10% XG 4%	Concentration-dependent model	61.9
	Rheology-informed model	41.1
Alginate 2% $CaCl_2$ 0.2%	Concentration-dependent model	73.4
	Rheology-informed model	27.5
Alginate 2% $CaCl_2$ 0.3%	Concentration-dependent model	93.2
	Rheology-informed model	24.3

Figure 7. Error map of the prediction of printing resolution with different concentrations of bioinks using (A) concentration-dependent model and (B) rheology-informed model. (C) Bar graph of errors in the prediction at each bioink composition. (D) Table of error values for different bioink formulations and prediction models.

the prediction of printing resolution with different concentrations of bioink components has proceeded with two machine learning models including CDML and RIHML. Specifically, the error maps in Figure 7A and B indicate the errors of predicted resolution compared to the actual resolution with various material concentrations, nozzle velocities, and nozzle types, using CDML and RIHML, respectively. Particularly, most regions of the error map of RIHML are bluish having low numbers of yellow squares with low prediction errors. Nevertheless, in the error map of the CDML, many yellow squares were observed with high prediction errors. For instance, the prediction of F127 45%, gelatin 10% combined with xanthan gum 4%, and alginate 2% crosslinked with $CaCl_2$ had significantly large errors with different nozzle types and speeds. Furthermore, for the prediction using CDML, the errors were more than 50% in 45 data and 75% in 27 data among the total data number of 96, which implies a high prediction error of this method. In contrast, the errors of only two data were over 75% at the F127 concentration of 45% using RIHML. Figure 7C and D visualize the average errors to compare the printing accuracy for each bioink composition. Further, the prediction using both machine learning models exhibited relatively high errors with the concentration of F127 of 45%, but the average error is approximately two times higher in CDML. The prediction with the rheology-informed hierarchical model exhibits less error than the concentration-based model in all the concentrations.

3.4.3. Prediction of the different bioink integrated with a new material

To demonstrate the prediction of the bioink incorporated with a new material, which is significantly challenging with current bioprinting prediction techniques, non-trained bioinks were prepared by mixing the alginate solution with CNC in two concentrations of 2.5% and 5%. Therefore, the model training proceeded without data on alginate/CNC composition as shown in **Table S1** (Supplementary File). Precisely, Figure 8A shows that 85 cases were collected with alginate/CNC composites to consist of a prediction dataset. More so, the predicted resolution of the new compositions and a fitted line of actual printing resolution are shown in Figure 8B and C. In the prediction results using CDML shown in Figure 8B, most of the predicted points in red color with alginate 2%/CNC 5% composition strayed from the defined resolution range from 0 to 4 mm. This result implies the difficulty of predicting printability when new materials are added to bioink. In comparison, all the prediction data using

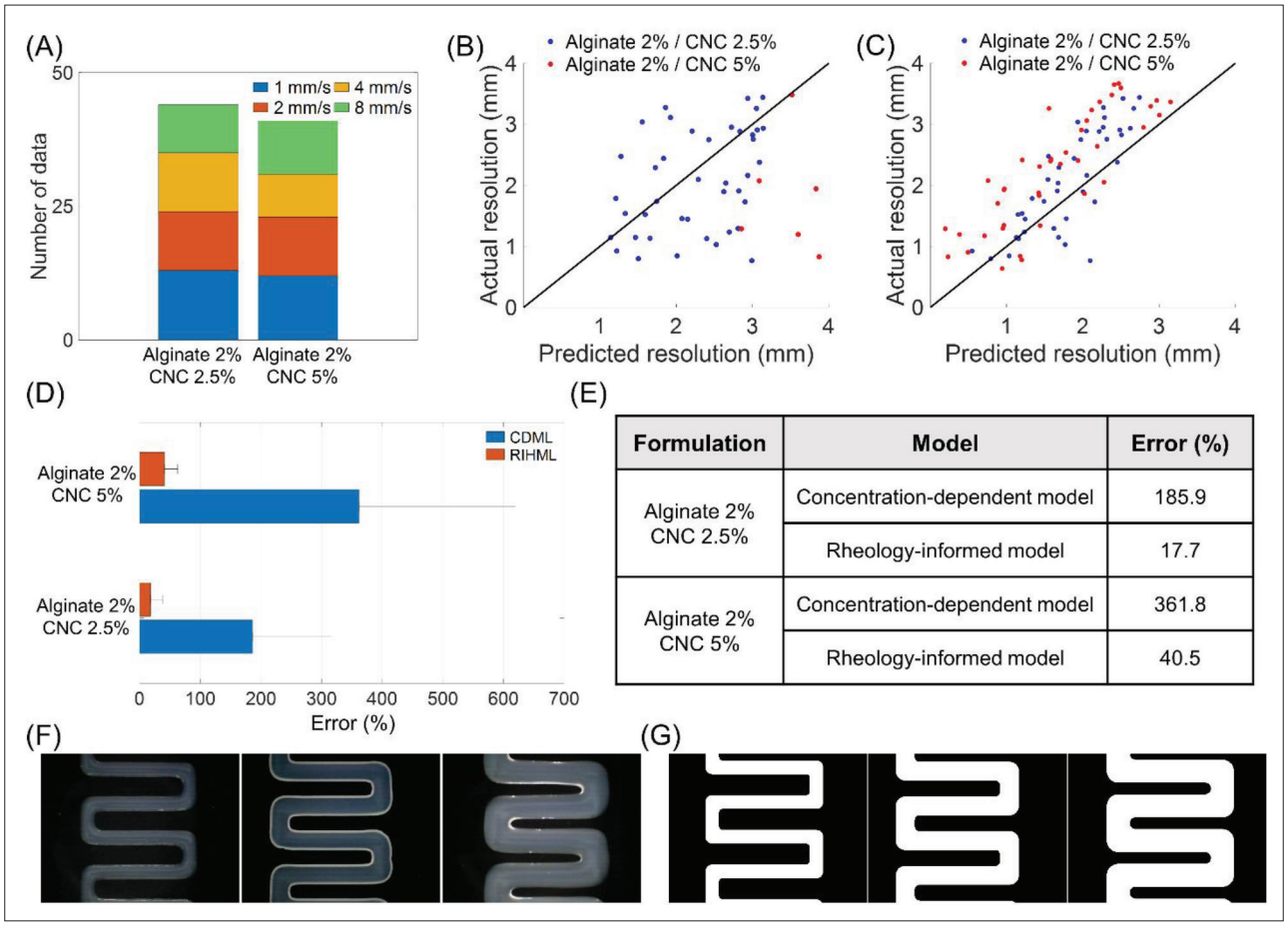

Formulation	Model	Error (%)
Alginate 2% CNC 2.5%	Concentration-dependent model	185.9
	Rheology-informed model	17.7
Alginate 2% CNC 5%	Concentration-dependent model	361.8
	Rheology-informed model	40.5

Figure 8. Prediction of printing resolution using the trained models with different concentrations of CNC incorporated with 2% alginate. (A) The number of results for alginate/CNC composition at different velocities. Fitting actual values with prediction values with (B) CDML and (C) RIHML. (D) Bar graph of average errors for each model. (E) Error values for different bioinks formulations and prediction models. Visual comparison between (F) actual image of printed alginate/CNC composition and (G) simulated image using the printing resolution predicted by RIHML. Abbreviations: CDML, concentration-dependent machine learning; CNC, cellulose nanocrystal; RIHML, rheology-informed hierarchical machine learning.

RIHML existed within the range of the axis as shown in Figure 8C. To quantitatively elucidate this phenomenon, Figure 8D and E can differentiate the average prediction accuracy between the concentration-dependent model and the rheology-informed model. The RIHML method can adequately predict the printing resolution of bioink with new material, but CDML predictions are unreliable and have significant errors. Specifically, the concentration-dependent model shows approximately 10-fold errors compared to the rheology-informed model using the same prediction dataset. This result implies the performance of RIHML is less affected by the bioink composition, even with new materials. Furthermore, to visually compare the strand size of actual printing and prediction using RIHML, the binary images of the printed scaffolds were created using simulation and compared with their actual images. Figure 8F shows actual images of the printed alginate/CNC scaffolds. The simulated images using the printing resolution of the alginate/CNC composition predicted by RIHML are presented in Figure 8G and agreed well with the actual images.

4. Discussion

This study reports the application of a rheology-informed hierarchical model to enhance the prediction accuracy of the printing resolution of constructs fabricated by extrusion-based bioprinting. Specifically, five different machine learning models, including the RIHML model as well as two classical machine learning models (RF and SVM) and the conventional models based on artificial neural networks (concentration-dependent model and printing parameter-dependent model), were trained and tested using a small dataset of bioink properties and printing parameters. More precisely, the models were used to predict the printing resolution in three different

cases, including new printing parameters with trained bioink materials, new concentrations of the trained bioink constituents, and untrained bioink compositions with the new material. For different nozzle velocities, the results of the study showed that the RIHML model exhibited the lowest error percentage (around 18%) in predicting the printing resolution. Additionally, the RIHML model showed low error (around 10%) in predicting the printing resolution for different pressures, which is 2-fold and 5-fold lower than CDML and PDML, respectively. Moreover, the printing resolution for different bioink concentrations was predicted, and it was demonstrated that the RIHML model exhibited lower error percentages than the CDML model for all the different concentrations of bioink constituents such as F127, gelatin, xanthan gum, and $CaCl_2$. Additionally, the machine learning models were used to predict the printing resolution with a new material (CNC) added to the alginate-based bioink, which is the most challenging among the three cases. The results of the study showed that RIHML can predict the printing resolution with reasonably low errors while the printing resolution was hardly predictable using CDML with considerably large errors.

Overall, the experimental results indicate that the rheology-informed hierarchical model can be a useful tool to predict the printing resolution of extrusion-based bioprinting. Furthermore, while other studies related to the prediction of printability in bioprinting could anticipate the printability changes only with limited parameters, such as bioink material properties or printing conditions, the RIHML model is versatile to predict the printing resolution in different conditions of varying printing parameters, varying material concentrations, and new bioink compositions[40,43,54]. Additionally, the neural network structure of RIHML is based on rheological properties, which can be widely obtained from most biomaterials, and it can be trained without significant alterations of the structure. Therefore, the RIHML model is adaptable and expandable compared to the conventional models, and the printing and rheological datasets may be accumulated to enhance the prediction accuracy.

Since the formulation of bioinks and the process of bioprinting are more complicated and correlated, the prediction of printability in 3D bioprinting has become more challenging. Recently, there have been attempts related to the prediction of bioprinting printability using machine learning. However, unlike other fields such as medical imaging and genetics, 3D bioprinting suffers from data size, which may hardly be large because the preparation of bioinks with various compositions and their 3D printing with multiple parameters are sequential and highly time-consuming[55-57]. Therefore, it is crucial to develop an efficient machine learning model that is suitable for small dataset sizes while ensuring high prediction accuracy. With the hierarchical architecture of the developed model, RIHML can effectively predict the printing resolution of extrusion-based bioprinting using small datasets. In this study, the dataset of 537 numbers of bioink rheological properties and printing process was used for training, validation, and testing of the machine learning model. Several bioprinting studies employed small datasets to optimize printing resolution and parameters using conventional machine learning skills, but their practical applications were limited due to low prediction accuracy, poor expandability, and low training efficiency[41,42,44,45]. However, the RIHML model can easily generalize and embrace new data, even with a small dataset size owing to its intrinsic features in the dataset that are not biased to specific bioink, but rather are general. Moreover, due to the potential of data accumulation, if various rheological and printing data are additionally collected in sufficient size for deep learning, prediction using a rheology-informed neural network with deeper hidden layers may be attempted.

Although the RIHML model has the potential for accurate and robust prediction of printability, there is still room for improvement. Due to the generalizability of the bioink properties, a wider range of rheological properties of bioinks can enhance the prediction accuracy of the RIHML model. For instance, in the results presented in Figure 7C, relatively high errors were observed in F127 with a concentration of 45%. Specifically, this may occur because its viscosity and storage modulus were the highest around the upper bound of the rheological data range. In terms of future work, it would be beneficial to further validate the performance of the RIHML model from other types of bioprinting methods, such as inkjet-based or laser-assisted bioprinting, to demonstrate the feasibility of rheology-based prediction of printability across different bioprinting methods. Additionally, future studies could investigate the potential of the RIHML model in predicting other aspects of printability, such as the extrudability, pore size, pore shape, and shape fidelity of the stacked layers.

5. Conclusion

In conclusion, this study suggests that the rheology-informed hierarchical model can be a useful tool for predicting the printing resolution of constructs fabricated by extrusion-based bioprinting. Interestingly, the RIHML model demonstrated the lowest errors (around 18%) in predicting the printing resolution for different printing parameters such as nozzle velocities and pressures,

compared to the conventional models such as the concentration-dependent model and printing parameter-dependent model. Additionally, the RIHML model also exhibited low error (around 10%) in predicting the printing resolution for different concentrations of bioink constituents, such as Pluronic F-127, gelatin, xanthan gum, and $CaCl_2$. Furthermore, the RIHML model can predict the printing resolution with a new nanomaterial (CNC) added to the alginate-based bioink, which is hardly possible with conventional methods. This study demonstrated the importance of considering the rheological properties of bioinks in predicting the printability of extrusion-based bioprinting and highlighted the potential of the RIHML model as a useful tool for predicting the printing resolution of extrusion-based bioprinting. In addition, the results indicate that the RIHML model can be versatile and expandable in the prediction of bioprinting resolution, and the printing and rheological datasets may be accumulated to enhance the prediction accuracy. The potential for the RIHML model to generalize and embrace new data, even with a small dataset size, is an advantage in the field of 3D bioprinting where data size is limited due to the complexity and time-consuming nature of the preparation of bioinks with various compositions and 3D printing with multiple parameters.

Acknowledgments

None.

Funding

This research was supported by a National Research Foundation of Korea (NRF) grant (NRF-2021R1I1A3040459) funded by the Korean government (MOE). This research was supported by a grant of the Korea Health Technology R&D Project through the Korea Health Industry Development Institute (KHIDI), funded by the Ministry of Health & Welfare, Republic of Korea (grant number : HI22C1323).

Conflict of interest

The authors declare no conflicts of interests.

Author contributions

Conceptualization: Dageon Oh, Seung Yun Nam
Data curation: Dageon Oh, Min Chang Kim
Formal analysis: Dageon Oh
Funding acquisition: Eun-Jae Chung, Seung Yun Nam
Investigation: Dageon Oh, Seung Yun Nam
Methodology: Dageon Oh, Seung Yun Nam
Project administration: Dageon Oh, Seung Yun Nam
Supervision: Seung Yun Nam
Validation: Dageon Oh
Visualization: Dageon Oh
Writing – original draft: Dageon Oh, Seung Yun Nam
Writing – review & editing: Masoud Shirzad, Eun-Jae Chung, Seung Yun Nam

Ethics approval and consent to participate

Not applicable.

Consent for publication

Not applicable.

Availability of data

The data presented in this study are available on request from the corresponding author.

References

1. Ozbolat, Yu Y, 2013, Bioprinting toward organ fabrication: Challenges and future trends. *IEEE Trans Biomed Eng,* 60(3): 691–699.

   https://doi.org/10.1109/TBME.2013.2243912

2. Murphy SV, Atala A, 2014, 3D bioprinting of tissues and organs. *Nat Biotechnol,* 32(8), 773–785.

   https://doi.org/10.1038/nbt.2958

3. Sun W, Starly B, Daly AC, *et al.*, 2020, The bioprinting roadmap. *Biofabrication,* 12(2): 022002.

   https://doi.org/10.1088/1758-5090/ab5158

4. Daly AC, Prendergast ME, Hughes AJ, *et al.*, 2021, Bioprinting for the biologist. *Cell,* 184(1): 18–32.

   https://doi.org/10.1016/j.cell.2020.12.002

5. Lu D, Yang Y, Zhang P, *et al.*, 2022, Development and application of three-dimensional bioprinting scaffold in the repair of spinal cord injury. *Tissue Eng Regen Med,* 19(6): 1113–1127.

   https://doi.org/10.1007/s13770-022-00465-1

6. Tan B, Gan S, Wang X, *et al.*, 2021, Applications of 3D bioprinting in tissue engineering: advantages, deficiencies, improvements, and future perspectives. *J Mater Chem B,* 9(27): 5385–5413.

   https://doi.org/10.1039/D1TB00172H

7. Mandrycky C, Wang Z, Kim K, *et al.*, 2016, 3D bioprinting for engineering complex tissues. *Biotechnol Adv,* 34(4): 422–434.

   https://doi.org/10.1016/j.biotechadv.2015.12.011

8. Yilmaz B, Al Rashid A, Mou YA, *et al.*, 2021, Bioprinting: A review of processes, materials and applications. *Bioprinting,* 23: e00148.

   https://doi.org/10.1016/j.bprint.2021.e00148

9. Mao X, Wang Z, 2022, Research progress of three-dimensional bioprinting artificial cardiac tissue. *Tissue Eng Regen Med,* 20: 1–9.

   https://doi.org/10.1007/s13770-022-00495-9

10. Jacob GT, Passamai VE, Katz S, *et al.*, 2022, Hydrogels for extrusion-based bioprinting: general considerations. *Bioprinting,* 27: e00212.

    https://doi.org/10.1016/j.bprint.2022.e00212

11. Merceron TK, Burt M, Seol Y-J, *et al.*, 2015, A 3D bioprinted complex structure for engineering the muscle–tendon unit. *Biofabrication,* 7(3): 035003.

    http://dx.doi.org/10.1088/1758-5090/7/3/035003

12. Melchels FP, Dhert WJ, Hutmacher DW, *et al.*, 2014, Development and characterisation of a new bioink for additive tissue manufacturing. *J Mater Chem B,* 2(16): 2282–2289.

    https://doi.org/10.1039/C3TB21280G

13. Ozbolat IT, Hospodiuk M, 2016, Current advances and future perspectives in extrusion-based bioprinting. *Biomaterials,* 76: 321–343.

    https://doi.org/10.1016/j.biomaterials.2015.10.076

14. Zhang YS, Haghiashtiani G, Hübscher T, *et al.*, 2021, 3D extrusion bioprinting. *Nat Rev Methods Primers,* 1(1): 75.

    https://doi.org/10.1038/s43586-021-00073-8

15. Ning L, Chen X, 2017, A brief review of extrusion-based tissue scaffold bio-printing. *Biotechnol J,* 12(8): 1600671.

    https://doi.org/10.1002/biot.201600671

16. Xuan Z, Peng Q, Larsen T, *et al.*, 2023, Tailoring hydrogel composition and stiffness to control smooth muscle cell differentiation in bioprinted constructs. *Tissue Eng Regen Med,* 20(2): 199–212.

    https://doi.org/10.1007/s13770-022-00500-1

17. Willson K, Ke D, Kengla C, *et al.*, 2020, Extrusion-based bioprinting: Current standards and relevancy for human-sized tissue fabrication. *Methods Mol Biol,* 2140: 65–92.

    https://doi.org/10.1007/978-1-0716-0520-2

18. Hölzl K, Lin S, Tytgat L, *et al.*, 2016, Bioink properties before, during and after 3D bioprinting. *Biofabrication,* 8(3): 032002.

    http://dx.doi.org/10.1088/1758-5090/8/3/032002

19. Chung JH, Naficy S, Yue Z, *et al.*, 2013, Bio-ink properties and printability for extrusion printing living cells. *Biomater Sci,* 1(7): 763–773.

    https://doi.org/10.1039/C3BM00012E

20. Jin Y, Chai W, Huang Y, 2017, Printability study of hydrogel solution extrusion in nanoclay yield-stress bath during printing-then-gelation biofabrication. *Mater Sci Eng C,* 80: 313–325.

    https://doi.org/10.1016/j.msec.2017.05.144

21. Datta P, Barui A, Wu Y, *et al.*, 2018, Essential steps in bioprinting: From pre-to post-bioprinting. *Biotechnol Adv,* 36(5): 1481–1504.

    https://doi.org/10.1016/j.biotechadv.2018.06.003

22. Sarker M, Naghieh S, McInnes AD, *et al.*, 2019, Bio-fabrication of peptide-modified alginate scaffolds: Printability, mechanical stability and neurite outgrowth assessments. *Bioprinting,* 14: e00045.

    https://doi.org/10.1016/j.bprint.2019.e00045

23. Gillispie G, Prim P, Copus J, *et al.*, 2020, Assessment methodologies for extrusion-based bioink printability. *Biofabrication,* 12(2): 022003.

    https://doi.org/10.1088/1758-5090/ab6f0d

24. Schwab A, Levato R, D'Este M, *et al.*, 2020, Printability and shape fidelity of bioinks in 3D bioprinting. *Chem Rev,* 120(19): 11028–11055.

    https://doi.org/10.1021/acs.chemrev.0c00084

25. Malekpour A, Chen X, 2022, Printability and cell viability in extrusion-based bioprinting from experimental, computational, and machine learning views. *J Funct Biomater,* 13(2): 40.

    https://doi.org/10.3390/jfb13020040

26. Ramesh S, Harrysson OL, Rao PK, *et al.*, 2021, Extrusion bioprinting: Recent progress, challenges, and future opportunities. *Bioprinting,* 21: e00116.

    https://doi.org/10.1016/j.bprint.2020.e00116

27. Kang K, Hockaday L, Butcher J, 2013, Quantitative optimization of solid freeform deposition of aqueous hydrogels. *Biofabrication,* 5(3): 035001.

    http://dx.doi.org/10.1088/1758-5082/5/3/035001

28. Tian S, Zhao H, Lewinski N, 2021, Key parameters and applications of extrusion-based bioprinting. *Bioprinting,* 23: e00156.

    https://doi.org/10.1016/j.bprint.2021.e00156

29. Naghieh S, Chen X, 2021, Printability–A key issue in extrusion-based bioprinting. *J Pharm Anal,* 11(5): 564–579.

    https://doi.org/10.1016/j.jpha.2021.02.001

30. Fu Z, Naghieh S, Xu C, *et al.*, 2021, Printability in extrusion bioprinting. *Biofabrication,* 13(3): 033001.

    https://doi.org/10.1088/1758-5090/abe7ab

31. Lee H, Yoo JM, Ponnusamy NK, *et al.*, 2022, 3D-printed hydroxyapatite/gelatin bone scaffolds reinforced with graphene oxide: Optimized fabrication and mechanical characterization. *Ceram Int,* 48(7): 10155–10163.

    https://doi.org/10.1016/j.ceramint.2021.12.227

32. Kim MH, Nam SY, 2020, Assessment of coaxial printability for extrusion-based bioprinting of alginate-based tubular constructs. *Bioprinting,* 20: e00092.

    https://doi.org/10.1016/j.bprint.2020.e00092

33. Song K, Zhang D, Yin J, *et al.*, 2021, Computational study of extrusion bioprinting with jammed gelatin microgel-based composite ink. *Addit Manuf,* 41: 101963.

https://doi.org/10.1016/j.addma.2021.101963

34. Leppiniemi J, Lahtinen P, Paajanen A, *et al.*, 2017, 3D-printable bioactivated nanocellulose–alginate hydrogels. *ACS Appl Mater Interfaces,* 9(26): 21959–21970.

https://doi.org/10.1021/acsami.7b02756

35. Kim MH, Lee YW, Jung W-K, *et al.*, 2019, Enhanced rheological behaviors of alginate hydrogels with carrageenan for extrusion-based bioprinting. *J Mech Behav Biomed Mater,* 98: 187–194.

https://doi.org/10.1016/j.jmbbm.2019.06.014

36. Göhl J, Markstedt K, Mark A, *et al.*, 2018, Simulations of 3D bioprinting: Predicting bioprintability of nanofibrillar inks. *Biofabrication,* 10(3): 034105.

https://doi.org/10.1088/1758-5090/aac872

37. Bonatti AF, Chiesa I, Vozzi G, *et al.*, 2021, Open-source CAD-CAM simulator of the extrusion-based bioprinting process. *Bioprinting,* 24: e00172.

https://doi.org/10.1016/j.bprint.2021.e00172

38. Suntornnond R, Tan EYS, An J, *et al.*, 2016, A mathematical model on the resolution of extrusion bioprinting for the development of new bioinks. *Materials,* 9(9): 756.

https://doi.org/10.3390/ma9090756

39. Bonatti AF, Vozzi G, Chua CK, *et al.*, A deep learning approach for error detection and quantification in extrusion-based bioprinting. *Mater Today: Proc,* 70: 131–135.

https://doi.org/10.1016/j.matpr.2022.09.006

40. Ruberu K, Senadeera M, Rana S, *et al.*, 2021, Coupling machine learning with 3D bioprinting to fast track optimisation of extrusion printing. *Appl Mater Today,* 22: 100914.

https://doi.org/10.1016/j.apmt.2020.100914

41. Lee J, Oh SJ, An SH, *et al.*, 2020, Machine learning-based design strategy for 3D printable bioink: Elastic modulus and yield stress determine printability. *Biofabrication,* 12(3): 035018.

https://doi.org/10.1088/1758-5090/ab8707

42. Conev A, Litsa EE, Perez MR, *et al.*, 2020, Machine learning-guided three-dimensional printing of tissue engineering scaffolds. *Tissue Eng Part A,* 26(23–24): 1359–1368.

https://doi.org/10.1089/ten.tea.2020.0191

43. Fu Z, Angeline V, Sun W, 2021, Evaluation of printing parameters on 3D extrusion printing of pluronic hydrogels and machine learning guided parameter recommendation. *Int J Bioprint,* 7(4): 179–189.

https://doi.org/10.18063%2Fijb.v7i4.434

44. Bone JM, Childs CM, Menon A, *et al.*, 2020, Hierarchical machine learning for high-fidelity 3D printed biopolymers. *ACS Biomater Sci Eng,* 6(12): 7021–7031.

https://doi.org/10.1021/acsbiomaterials.0c00755

45. Menon A, Póczos B, Feinberg AW, *et al.*, 2019, Optimization of silicone 3D printing with hierarchical machine learning. *3D Print Addit Manuf,* 6(4): 181–189.

https://doi.org/10.1089/3dp.2018.0088

46. Jin Z, Zhang Z, Shao X, *et al.*, 2021, Monitoring anomalies in 3D bioprinting with deep neural networks. *ACS Biomater Sci Eng*, 9(7): 3945–3952.

https://doi.org/10.1021/acsbiomaterials.0c01761

47. Mancha Sánchez E, Gómez-Blanco JC, López Nieto, *et al.*, 2020, Hydrogels for bioprinting: A systematic review of hydrogels synthesis, bioprinting parameters, and bioprinted structures behavior. *Front Bioeng Biotechnol,* 8: 776.

https://doi.org/10.3389/fbioe.2020.00776

48. Zhang Z, Jin Y, Yin J, *et al.*, 2018, Evaluation of bioink printability for bioprinting applications. *Appl Phys Rev,* 5(4): 041304.

https://doi.org/10.1063/1.5053979

49. Chimene D, Lennox KK, Kaunas RR, *et al.*, 2016, Advanced bioinks for 3D printing: A materials science perspective. *Annal Biomed Eng,* 44(6): 2090–2102.

https://doi.org/10.1007/s10439-016-1638-y

50. Cooke ME, Rosenzweig DH, 2021, The rheology of direct and suspended extrusion bioprinting. *APL Bioeng,* 5(1): 011502.

https://doi.org/10.1063/5.0031475

51. Paxton N, Smolan W, Böck T, *et al.*, 2017, Proposal to assess printability of bioinks for extrusion-based bioprinting and evaluation of rheological properties governing bioprintability. *Biofabrication,* 9(4): 044107.

https://doi.org/10.1088/1758-5090/aa8dd8

52. Ouyang L, Yao R, Zhao Y, *et al.*, 2016, Effect of bioink properties on printability and cell viability for 3D bioplotting of embryonic stem cells. *Biofabrication,* 8(3): 035020.

http://dx.doi.org/10.1088/1758-5090/8/3/035020

53. Xu X, Jagota A, Peng S, *et al.*, 2013, Gravity and surface tension effects on the shape change of soft materials. *Langmuir,* 29(27): 8665–8674.

https://doi.org/10.1021/la400921h

54. Gao T, Gillispie GJ, Copus JS, *et al.*, 2018, Optimization of gelatin–alginate composite bioink printability using rheological parameters: A systematic approach. *Biofabrication,* 10(3): 034106.

https://doi.org/10.1088/1758-5090/aacdc7

55. Yu C, Jiang J, 2020, A perspective on using machine learning in 3D bioprinting. *Int J Bioprint,* 6(1): 4–11.

https://doi.org/10.18063%2Fijb.v6i1.253

56. Shin J, Lee Y, Li Z, *et al.*, 2022, Optimized 3D bioprinting technology based on machine learning: A review of recent trends and advances. *Micromachines,* 13(3): 363.

https://doi.org/10.3390/mi13030363

57. Ng WL, Chan A, Ong YS, *et al.*, 2020, Deep learning for fabrication and maturation of 3D bioprinted tissues and organs. *Virtual Phys Prototyp,* 15(3): 340–358.

https://doi.org/10.1080/17452759.2020.1771741